Progress in Photovoltaics: Research and Applications

WILEY

PROGRESS IN PHOTOVOLTAICS

SHORT COMMUNICATION OPEN ACCESS

Solar Cell Efficiency Tables (Version 66)

Martin A. Green[1] | Ewan D. Dunlop[2] | Masahiro Yoshita[3] | Nikos Kopidakis[4] | Karsten Bothe[5] | Gerald Siefer[6] | Xiaojing Hao[1] | Jessica Yajie Jiang[1]

[1]Australian Centre for Advanced Photovoltaics, School of Photovoltaic and Renewable Energy Engineering, University of New South Wales, Sydney, Australia | [2]European Commission – Joint Research Centre, Ispra, Varese, Italy | [3]Renewable Energy Research Center (RENRC), National Institute of Advanced Industrial Science and Technology (AIST), Tsukuba, Ibaraki, Japan | [4]National Renewable Energy Laboratory, Golden, Colorado, USA | [5]Calibration and Test Center (CalTeC), Solar Cells Laboratory, Institut für Solarenergieforschung GmbH (ISFH), Emmerthal, Germany | [6]Fraunhofer-Institute for Solar Energy Systems – ISE, Freiburg, Germany

Correspondence: Martin A. Green (m.green@unsw.edu.au)

Received: 4 April 2025 | **Revised:** 9 April 2025 | **Accepted:** 14 April 2025

Funding: This study was supported by the Australian Renewable Energy Agency (SRI-001); the US Department of Energy (Office of Science, Office of Basic Energy Sciences and Energy Efficiency and Renewable Energy, Solar Energy Technology Program) (DE-AC36-08-GO28308); and the Ministry of Economy, Trade and Industry.

Keywords: energy conversion efficiency | photovoltaic efficiency | solar cell efficiency

ABSTRACT

Consolidated tables showing an extensive listing of the highest independently confirmed efficiencies for solar cells and modules are presented. Guidelines for inclusion of results into these tables are outlined, and new entries since January 2025 are reviewed.

1 | Introduction

Since January 1993, *Progress in Photovoltaics* has published six monthly listings of the highest confirmed efficiencies for a range of photovoltaic cell and module technologies [1–3]. By providing guidelines for inclusion of results into these tables, this not only provides an authoritative summary of the current state of the art but also encourages researchers to seek independent confirmation of results and to report results on a standardised basis. In Version 33 of these tables, results were updated to the new internationally accepted reference spectrum (International Electrotechnical Commission IEC 60904-3, Ed. 2, 2008).

The most important criterion for inclusion of results into the tables is that they must have been independently measured by a recognised test centre listed in Versions 61 and 62 (also updated in 64). A distinction is made between three different eligible definitions of cell area: total area, aperture area and designated illumination area, as also defined elsewhere [2] (note that, if masking is used, masks must have a simple aperture geometry, such as square, rectangular or circular—masks with multiple openings are not eligible). 'Active area' efficiencies are not included. There are also certain minimum values of the area sought for the different device types (above 0.05 cm^2 for a concentrator cell or one-sun 'notable exception', 1 cm^2 for a one-sun cell, 200 cm^2 for a 'submodule' and 800 cm^2 for a module).

Tabled results are reported for cells and modules made from different semiconductors and for sub-categories within each semiconductor grouping. From Version 36 onwards, spectral response information is included (when possible) in the form of a plot of the external quantum efficiency (EQE) versus wavelength, either as absolute values or normalised to the peak measured value. Current–voltage (I–V) curves have also been included where possible from Version 38 onwards.

Three notable changes are being introduced in this issue. For large (> 150 cm^2), commercially sized 1 Sun silicon cells, as well as the best outright result, the best result measured on a 'total area' basis only will be included for the different competing commercial technologies as "notable exceptions". Also, the minimum area acceptable for other 1 Sun 'notable exceptions' is 0.05

TABLE 1 | Confirmed single-junction terrestrial cell and submodule efficiencies measured under the global AM1.5 spectrum (1000 W/m^2) at 25 °C (IEC 60904–3:2008 or ASTM G-173-03 global).

Classification	Efficiency (%)	Area (cm^2)	V_{oc} (V)	J_{sc} (mA/cm^2)	Fill factor (%)	Test centre (date)	Description
Silicon							
Si (crystalline cell)	27.4 ± 0.4[a]	165.72 (t)	0.7456	42.35[b]	86.7	ISFH (9/24)	LONGi, n-type HTBC [4]
Si (crystalline cell)	**27.8 ± 0.4[a]**	**133.63 (da)**	**0.7449**	**42.64[c]**	**87.5**	**ISFH (1/25)**	**LONGi, n-type HTBC [4]**
Si (thin-film minimodule)	10.5 ± 0.3	94.0 (ap)	0.492[d]	29.7[d,e]	72.1	FhG-ISE (8/07)	CSG Solar (<2 μm on glass) [5]
III–V cells							
GaAs (thin-film cell)	29.1 ± 0.6	0.998 (ap)	1.1272	29.78[f]	86.7	FhG-ISE (10/18)	Alta Devices [6]
InP (crystalline cell)	24.2 ± 0.5[g]	1.008 (ap)	0.939	31.15[h]	82.6	NREL (3/13)	NREL [7]
Thin film chalcogenide							
CIGS (cell) (Cd-free)	23.35 ± 0.5	1.043 (da)	0.734	39.58[i]	80.4	AIST (11/18)	Solar Frontier [8]
CIGSSe (submodule)	20.3 ± 0.4	526.7 (ap)	0.6834	39.55[d,j]	75.1	NREL (5/23)	Avancis, 100 cells [9]
CdTe (cell)	21.0 ± 0.4	1.0623 (ap)	0.8759	30.25[k]	79.4	Newport (8/14)	First Solar, on glass [10]
CZTSSe (cell)	**14.1 ± 0.3**	**1.075 (da)**	**0.5356**	**40.67[c]**	**69.7**	**NPVM (1/25)**	**IoP/CAS [11]**
CZTSSe (minimodule)	11.95 ± 0.3	10.47 (da)	0.5073[d]	34.82[b,d]	67.7	NPVM (9/24)	IoP/CAS, 4 cells [11]
CZTS (cell)	10.0 ± 0.2	1.113 (da)	0.7083	21.77[h]	65.1	NREL (3/17)	UNSW [12]
Amorphous/microcrystalline							
Si (amorphous cell)	10.2 ± 0.3[g,l]	1.001 (da)	0.896	16.36[k]	69.8	AIST (7/14)	AIST [13]
Si (microcrystalline cell)	11.9 ± 0.3[g]	1.044 (da)	0.550	29.72[h]	75.0	AIST (2/17)	AIST [14]
Perovskite							
Perovskite (cell)	**26.9 ± 0.8[m]**	**1.017 (da)**	**1.203**	**27.13[c]**	**82.3**	**NPVM (3/25)**	**Soochow/UNSW/ BaimaLake [15]**
Perovskite (minimodule)	**23.9 ± 0.5[m]**	**19.48 (da)**	**1.070[d]**	**27.08[c,d]**	**82.6**	**NPVM (3/25)**	**Microquanta, 9 cells [16]**
Perovskite (submodule)	20.6 ± 0.7[m]	215.53 (da)	1.185[d]	22.22[b,d]	78.3	FhG-ISE (4/24)	KRICT/UniTest, 29 cells [17]

(Continues)

TABLE 1 | (Continued)

Classification	Efficiency (%)	Area (cm^2)	V_{oc} (V)	J_{sc} (mA/cm^2)	Fill factor (%)	Test centre (date)	Description
Dye sensitised							
Dye (cell)	11.9 ± 0.4[n]	1.005 (da)	0.744	22.47[o]	71.2	AIST (9/12)	Sharp [18, 19]
Dye (minimodule)	10.7 ± 0.4[n]	26.55 (da)	0.754[d]	20.19[d,p]	69.9	AIST (2/15)	Sharp, 7 serial cells [18, 19]
Dye (submodule)	8.8 ± 0.3[n]	398.8 (da)	0.697[d]	18.42[d,q]	68.7	AIST (9/12)	Sharp, 26 serial cells [18, 19]
Organic							
Organic (cell)	15.8 ± 0.3[g,r]	1.064 (da)	0.8513	25.11[s]	73.9	FhG-ISE (6/23)	Fraunhofer ISE/FMF [20]
Organic (minimodule)	15.7 ± 0.3[r]	19.31(da)	0.8771[d]	24.37[d,j]	73.4	JET (1/23)	ZhejiangU, 7 cells [21]
Organic (submodule)	14.5 ± 0.2[r]	204.11 (da)	0.8315[d]	23.32[d,s]	74.6	FhG-ISE (11/23)	FAU/FZJ, 38 cells [22]

Abbreviations: (ap), aperture area; (da), designated illumination area; (t), total area; AIST, Japanese National Institute of Advanced Industrial Science and Technology; CZTS, Cu_2ZnSnS_4; CZTSSe, $Cu_2ZnSnS_{4-y}Se_y$; CIGS, $CuIn_{1-y}Ga_ySe_2$; FhG-ISE, Fraunhofer Institut für Solare Energiesysteme; ISFH, Institute für Solarenergieforschung; JET, Japan Electrical Safety and Environment Technology Laboratories; NPVM, Chinese National Photovoltaic Industry Measurement and Testing Center; NREL, US National Renewable Energy Laboratory.

[a]Contacting: front: unmetallised; rear: rear 2 × 9BB, busbar resistance neglecting (brn) contacting, highly reflective (white) chuck (hrc).

[b]Spectral response and current–voltage curve reported in Version 65 of these tables.

[c]Spectral response and current–voltage curve reported in the present version of these tables.

[d]Reported on a 'per cell' basis.

[e]Recalibrated from original measurement.

[f]Spectral response and current–voltage curve reported in Version 53 of these tables.

[g]Not measured at an external laboratory.

[h]Spectral response and current–voltage curve reported in Version 50 of these tables.

[i]Spectral response and current–voltage curve reported in Version 54 of these tables.

[j]Spectral response and current–voltage curve reported in Version 62 of these tables.

[k]Spectral response and current–voltage curve reported in Version 45 of these tables.

[l]Stabilized by 1,000 hours exposure to 1 sun light at 50 C.

[m]Initial performance. References [23, 24] review the stability of similar devices.

[n]Initial efficiency. Reference [25] reviews the stability of similar devices.

[o]Spectral response and current–voltage curve reported in Version 41 of these tables.

[p]Spectral response and current–voltage curve reported in Version 46 of these tables.

[q]Spectral response and current–voltage curve reported in Version 43 of these tables.

[r]Initial performance. References [26, 27] review the stability of similar devices.

[s]Spectral response and current–voltage curve reported in Version 64 of these Tables.

TABLE 2 | 'Notable exceptions' for single-junction cells and submodules: 'Top dozen' confirmed results, not class records, measured under the global AM1.5 spectrum (1000 Wm^{-2}) at 25°C (IEC 60904-3:2008 or ASTM G-173-03 global).

Classification	Efficiency (%)	Area (cm^2)	V_{oc} (V)	J_{sc} (mA/cm^2)	Fill Factor (%)	Test centre (date)	Description
Cells (silicon)							
Si (PERC)	25.0 ± 0.5	4.00 (da)	0.706	42.7[a]	82.8	Sandia (3/99)	UNSW, p-type [28]
Si (p-TOPCon)	26.0 ± 0.5[b]	4.015 (da)	0.7323	42.05[c]	84.3	FhG-ISE (11/19)	FhG-ISE, p-type [29]
Si (p-TBC)	26.1 ± 0.3[b]	3.9857 (da)	0.7266	42.62[d]	84.3	ISFH (2/18)	ISFH, p-type [30]
Si (large PERC)	**24.1 ± 0.4[e]**	**441.3 (t)**	**0.6997**	**41.79[f]**	**82.3**	**ISFH (12/24)**	**Trina p-type [31]**
Si (large TOPCon)	**26.4 ± 0.4[g]**	**334.9 (t)**	**0.7412**	**42.38[f]**	**84.0**	**ISFH (5/25)**	**Jinko, n-type [32]**
Si (large TBC)	27.0 ± 0.5[h]	350.0 (t)	0.7447	42.32[i]	85.8	ISFH (8/24)	LONGi, n-type [4]
Si (large HJT)	26.8 ± 0.4[j]	274.4 (t)	0.7514	41.45[k]	86.1	ISFH (10/22)	LONGi, n-type [33]
Si (large p-HJT)	26.6 ± 0.4[j]	274.1 (t)	0.7513	41.30[k]	85.6	ISFH (10/22)	LONGi, p-type [34]
Cells (chalcogenide)							
CIGS	23.6 ± 0.4	0.899 (da)	0.7671	38.30[l]	80.5	FhG-ISE (1/23)	Evolar/UppsalaU [35]
CdTe	23.1 ± 0.3	0.4507 (da)	0.9048	31.66[i]	80.6	NREL (5/24)	First Solar [36]
CZTSSe	**15.8 ± 0.3**	**0.2250 (da)**	**0.5540**	**38.14[f]**	**74.7**	**NPVM (1/25)**	**IoP/CAS [11]**
Cells (other)							
Perovskite	**27.3 ± 0.6[m]**	**0.1065 (da)**	**1.200**	**26.34[f]**	**85.4**	**NPVM (5/25)**	**Soochow/UNSW/ BaimaLake [15]**
Dye sensitised	13.0 ± 0.4[n]	0.1155 (da)	1.0396	15.55[l]	80.4	FhG-ISE (10/20)	EPFL [37]

Abbreviations: (ap), aperture area; (da), designated illumination area; (t), total area; AIST, Japanese National Institute of Advanced Industrial Science and Technology, CIGS, $CuIn_{1-y}Ga_ySe_2$; CZTS = Cu_2ZnSnS_4; CZTSSe, $Cu_2ZnSnS_{4-y}Se_y$; FhG-ISE, Fraunhofer-Institut für Solare Energiesysteme; ISFH, Institute for Solar Energy Research, HamelinNREL; National Renewable Energy Laboratory.

[a]Spectral response reported in Version 36 of these tables.

[b]Not measured at an external laboratory.

[c]Spectral response and current–voltage curves reported in Version 55 of these tables.

[d]Spectral response and current–voltage curve reported in Version 52 of these tables.

[e]Contacting: front: BB0, grn; rear: BB16, full area contacting (fac), grn.

[f]Spectral response and current–voltage curves reported in the present version of these tables.

[g]Contacting: 16BB, busbar resistance neglecting (brn); rear: 10 continuous + 10 dashed BBs, grid resistance neglecting (grn) contacting, highly reflective gold chuck (hrc).

[h]Contacting: front: unmetallised; rear: rear: 2x9BB, busbar resistance neglecting (brn) contacting, highly reflective (white) chuck (hrc).

[i]Spectral response and current–voltage curves reported Version 65 of these tables.

[j]Contacting: front: 12BB, busbar resistance neglecting (brn) contacting; rear: 12BB, grid resistance neglecting (grn) contacting, highly reflective chuck (hrc).

[k]Spectral response and current–voltage curves reported in Version 61 of these tables.

[l]Spectral response and current–voltage curves reported in Version 62 of these tables.

[m]Stability not investigated. References [23, 24] document stability of similar devices.

[n]Long term stability not investigated. Reference [25] documents stability of similar devices.

TABLE 3 | Confirmed non-concentrating, terrestrial high-bandgap cell efficiencies measured under the global AM1.5 spectrum (1000 Wm^{-2}) at 25°C (IEC 60904-3:2008 or ASTM G-173-03 global).

Classification	E_G (eV)	Efficiency (%)	Area (cm^2)	V_{oc} (V)	J_{sc} (mA/cm^2)	Fill Factor (%)	Test centre (date)	Description
1.55–1.65 eV								
Cu (Ga,In)S_2	**1.53**	**15.5 ± 0.3**	**0.4334 (ap)**	**0.920**	**23.41[a]**	**72.2**	**FhG-ISE (2015)**	**Showa Shell [38]**
Perovskite[b]	**1.57**	24.2 ± 0.8	0.0955 (ap)	1.1948	24.16[c]	84.0	Newport (1/19)	KRICT [39]
CZTS	**1.59**	13.2 ± 0.3	**0.2023(da)**	**0.8342**	**22.16[d]**	**71.6**	NPVM (5/24)	UNSW (Cd-free) [40]
Cu (Ga,In)S_2	**1.61**	**14.8 ± 0.9**	**0.3904 (da)**	**0.981**	**21.09[a]**	**71.6**	**FhG-ISE (9/23)**	**U.Luxembourg [41]**
1.65–1.75 eV								
Perovskite[b]	**1.65**	**16.2 ± 0.6**	**<0.2 (da)**	**1.1085**	**19.65[c]**	**74.2**	**Newport (12/13)**	**KRICT [42]**
$CuGaSe_2$:Al	**1.67**	**12.25 ± 0.3[e]**	**0.4990 (da)**	**0.959**	**17.63[a]**	**72.5**	**AIST (1/24)**	**AIST [43]**
1.75–1.85 eV								
GaInP	**1.82**	22.0 ± 0.3[e]	0.2502 (ap)	1.4695	16.63[f]	90.2	NREL (1/19)	NREL, rear HJ, strained AlInP [44]

Abbreviations: (ap), aperture area; (da), designated illumination area; (t), total area; AIST, Japanese National Institute of Advanced Industrial Science and Technology; Cu (Ga,In)S_2, $CuGa_{1-y}In_yS_2$; CZTS, Cu_2ZnSnS_4; FhG-ISE, Fraunhofer-Institut für Solare Energiesysteme; NPVM, Chinese National Photovoltaic Industry Measurement and Testing Center; NREL, National Renewable Energy Laboratory.

[a]Spectral response and current–voltage curves reported in the present version of these tables.

[b]Stability not investigated. References [23, 24] document stability of similar devices.

[c]Spectral response and more information reported in Reference [41].

[d]Spectral response and current–voltage curves reported in Version 65 of these tables.

[e]Not measured at an external laboratory.

[f]Spectral response and current–voltage curve reported in Version 54 of these Tables.

TABLE 4 | Confirmed multiple-junction terrestrial cell and submodule efficiencies measured under the global AM1.5 spectrum (1000 W/m^2) at 25°C (IEC 60904-3:2008 or ASTM G-173-03 global).

Classification	Efficiency (%)	Area (cm^2)	Voc (V)	Jsc (mA/cm^2)	Fill factor (%)	Test centre (date)	Description
III–V Multijunctions							
5 junction cell (bonded)	38.8 ± 1.2	1.021 (ap)	4.767	9.564	85.2	NREL (7/13)	Spectrolab, 2-terminal [45]
(2.17/1.68/1.40/1.06/.73 eV)							
InGaP/GaAs/InGaAs	37.9 ± 1.2	1.047 (ap)	3.065	14.27[a]	86.7	AIST (2/13)	Sharp, 2 term [46].
GaInP/GaAs (monolithic)	32.8 ± 1.4	1.000 (ap)	2.568	14.56[b]	87.7	NREL (9/17)	LG Electronics, 2 term.
III–V/Si Multijunctions							
GaInP/GaInAsP//Si (bonded)	36.1 ± 1.3[c]	3.987 (ap)	3.309	12.70[d]	86.0	FhG-ISE (5/23)	FhG-ISE/AMOLF, 2-term [47].
GaInP/GaAs/Si (mech. stack)	35.9 ± 0.5[c]	1.002 (da)	2.52/0.681	13.6/11.0	87.5/78.5	NREL (2/17)	NREL/CSEM/EPFL, 4-term [48].
GaInP/GaAs/Si (monolithic)	25.9 ± 0.9[c]	3.987 (ap)	2.647	12.21[e]	80.2	FhG-ISE (6/20)	Fraunhofer ISE, 2-term [49].
GaAsP/Si (monolithic)	23.4 ± 0.3	1.026 (ap)	1.732	17.34[f]	77.7	NREL (5/20)	OSU/UNSW/SolAero, 2-term [50]
GaAs/Si (mech. stack)	32.8 ± 0.5[c]	1.003 (da)	1.09/0.683	28.9/11.1[g]	85.0/79.2	NREL (12/16)	NREL/CSEM/EPFL, 4-term [48].
GaInP/GaInAs/Ge; Si (spectral split minimodule)	34.5 ± 2.0	27.83 (ap)	2.66/0.65	13.1/9.3	85.6/79.0	NREL (4/16)	UNSW/Azur/Trina, 4-term [51].
Perov./Si multijunctions							
Perovskite/Si	**34.85 ± 0.3[h]**	**1.0049(da)**	**1.997**	**21.08[i]**	**82.8**	**NREL (5/24)**	**LONGi, 2-term [52].**
Perovskite/Si (large)	**33.0 ± 0.5[h]**	**260.9(ap)**	**2.007**	**19.37[i]**	**84.8**	**NREL (4/25)**	**LONGi, 2-term [53].**
Perovskite/Si (large)	**28.6 ± 1.5[h]**	**330.56(t)**	**1.903**	**18.94[i]**	**79.3**	**FhG-ISE (11/24)**	**HanwhaQCells, 2-term [54].**
Other multijunctions							
Perovskite/CIGS	**24.6 ± 1.1[h]**	**1.110 (da)**	**1.762**	**19.28[i]**	**72.5**	**FhG-ISE (12/24)**	**HZB, 2-terminal [55]**
Perovskite/perovskite	28.2 ± 0.5[h]	1.038(da)	2.159	16.59[j]	78.9	JET (12/22)	NanjingU/Renshine, 2-term [56].
Perovskite/perovskite (minimodule)	**26.2 ± 0.6[h]**	**64.84(da)**	**2.182**	**15.60[i]**	**77.4**	**JET (9/24)**	**Renshine/NanjingU, 14 cells [57]**
a-Si/nc-Si/nc-Si (thin-film)	14.0 ± 0.4[c,k]	1.045 (da)	1.922	9.94[l]	73.4	AIST (5/16)	AIST, 2-term [58].
a-Si/nc-Si (thin-film)	12.7 ± 0.4[c,k]	1.000(da)	1.342	13.45[m]	70.2	AIST (10/14)	AIST, 2-term [59].

(Continues)

TABLE 4 | (Continued)

Classification	Efficiency (%)	Area (cm^2)	Voc (V)	Jsc (mA/cm^2)	Fill factor (%)	Test centre (date)	Description
'Notable exceptions'							
GaInP/GaAs (mqw)	32.9 ± 0.5[c]	0.250 (ap)	2.500	15.36[n]	85.7	NREL (1/20)	NREL/UNSW, multiple QW [60]
GaInP/GaAs/GaInAs	37.8 ± 1.4	0.998 (ap)	3.013	14.60[n]	85.8	NREL (1/18)	Microlink (ELO) [61]
GaInP/GaAs (mqw)/GaInAs	39.5 ± 0.5[c]	0.242 (ap)	2.997	15.44[o]	85.3	NREL (9/21)	NREL, multiple QW
6 junction (monolithic) (2.19/1.76/1.45/1.19/0.97/.7 eV)	39.2 ± 3.2[c]	0.247 (ap)	5.549	8.457[p]	83.5	NREL (11/18)	NREL, inv. metamorphic [62]
GaInP/AlGaAs/CIGS	28.1 ± 1.2[c]	0.1386(da)	2.952	11.72[q]	81.1	AIST (1/21)	AIST/FhG-ISE, 2-term [63].
Perovskite/perovskite	30.1 ± 0.8[h]	0.0493(da)	2.20	16.72[r]	81.8	JET (10/23)	NanjingU/Renshine, 2-term [56].

Abbreviations: (ap), aperture area; (da), designated illumination area; (t), total area; a-Si, amorphous silicon/hydrogen alloy; AIST, Japanese National Institute of Advanced Industrial Science and Technology; ESTI, European Solar Test Installation; FhG-ISE, Fraunhofer Institut für Solare Energiesysteme; JET, Japan Electrical Safety and Environment Technology Laboratories; nc-Si, nanocrystalline or microcrystalline silicon; NREL, US National Renewable Energy Laboratory.

[a]Spectral response and current–voltage curve reported in Version 42 of these tables.
[b]Spectral response and current–voltage curve reported in the Version 51 of these tables.
[c]Not measured at an external laboratory.
[d]Spectral response and current–voltage curves reported in the present version of these tables.
[e]Spectral response and current–voltage curve reported in Version 57 of these tables.
[f]Spectral response and current–voltage curve reported in Version 56 of these tables.
[g]Spectral response and current–voltage curve reported in Version 52 of these tables.
[h]Initial efficiency. References [23, 24] review the stability of similar perovskite-based devices.
[i]Spectral response and current–voltage curves reported in the present version of these tables.
[j]Spectral response and current–voltage curve reported in Version 63 of these tables.
[k]Stabilized by 1000 h exposure to 1 sun light at 50 C.
[l]Spectral response and current–voltage curve reported in Version 49 of these tables.
[m]Spectral responses and current–voltage curve reported in Version 45 of these tables.
[n]Spectral response and current–voltage curve reported in Version 53 of these tables.
[o]Spectral response and current–voltage curves reported in Version 59 of these tables.
[p]Spectral response and current–voltage curve reported in Version 54 of these Tables.
[q]Spectral response and current–voltage curve reported in Version 58 of these Tables.
[r]Spectral response and current–voltage curve reported in Version 64 of these tables.

TABLE 5 | Confirmed non-concentrating terrestrial module efficiencies measured under the global AM1.5 spectrum (1000 W/m^2) at a cell temperature of 25°C (IEC 60904-3:2008 or ASTM G-173-03 global).

Classification	Effic. (%)	Area (cm^2)	V_{oc} (V)	I_{sc} (A)	FF (%)	Test Centre (date)	Description
Si (crystalline)	**26.0 ± 0.3**	**18,156 (da)**	**40.38**	**13.896[d]**	**84.0**	**NREL (12/24)**	**LONGi, HBC [4]**
Si (crystalline)	**25.4 ± 0.4**	**16,279 (ap)**	**56.09**	**8.58[a]**	**86.0**	**FhG-ISE (12/24)**	**Trina, HJT [64]**
GaAs (thin-film)	25.1 ± 0.8	866.45 (ap)	11.08	2.303[b]	85.3	FhG-ISE (11/17)	Alta Devices [65]
CIGS (Cd-free)	19.2 ± 0.5	841 (ap)	48.0	0.456[c]	73.7	AIST (1/17)	Solar Frontier (70 cells) [66]
CdTe (thin-film)	19.9 ± 0.3	23,932 (da)	231.5	2.675[a]	77.1	NREL (6/23)	First Solar [67]
Perovskite	19.2 ± 0.4[e]	1027 (da)	59.4	0.4307[d]	77.1	NREL (12/23)	SolaEon [68]
Organic	13.1 ± 0.3[f]	1475 (da)	48.10	0.6015[g]	67.0	NREL (5/23)	Waystech/Nanobit [69]
Multijunction							
InGaP/GaAs/InGaAs	32.65 ± 0.7	965 (da)	24.30	1.520[h]	85.3	AIST (2/22)	Sharp (40 cells; 8 series) [70]
Perovskite/Si	**30.6 ± 1.3[e]**	**1185.6 (da)**	**11.783**	**3.578[a]**	**86.1**	**FhG-ISE (4/25)**	**Trina [52]**
Perovskite/Si (large)	26.9 ± 1.0[e]	16,023 (da)	56.18	9.456[d]	81.1	FhG-ISE (6/24)	Oxford PV [71]
a-Si/nc-Si (tandem)	12.3 ± 0.3[i]	14,322 (t)	280.1	0.902[j]	69.9	ESTI (9/14)	TEL Solar, Trubbach Labs [72]
'Notable Exceptions'							
CIGS (large)	18.6 ± 0.6	10,858 (ap)	58.00	4.545[k]	76.8	FhG-ISE (10/19)	Miasole [73]
InGaP/GaAs//Si	33.7 ± 0.7	775 (da)	20.3/2.83	1.25/1.93[g]	86.5/78.0	AIST (2/23)	Sharp/Toyota TI, 4-term [74].
InGaP/GaAs//CIGS	31.2 ± 0.7	778 (ap)	20.3/16.9	1.24/.26[g]	85.7/59.8	AIST (2/23)	Sharp/Idemitsu, 4-term [74].
Perovskite (large)	**18.1 ± 0.6[e]**	**7218 (t)**	**93.56**	**1.876[a]**	**74.4**	**NREL (1/25)**	**UtmoLight [75]**

Abbreviations: (ap), aperture area; (da), designated illumination area; (t), total area; a-Si, amorphous silicon/hydrogen alloy; a-SiGe, amorphous silicon/germanium/hydrogen alloy; CIGSS, CuInGaSSe; Effic., efficiency; FF, fill factor; nc-Si, nanocrystalline or microcrystalline silicon.

[a]Spectral response and current-voltage curve reported in the present version of these tables.
[b]Spectral response and current-voltage curve reported in Version 51 of these tables.
[c]Spectral response and current-voltage curve reported in Version 50 of these tables.
[d]Spectral response and current-voltage curve reported in Version 65 of these tables.
[e]Initial performance. References [25] and [26] review the stability of similar devices.
[f]Initial performance. References [28] and [29] review the stability of similar devices.
[g]Spectral response and current voltage curve reported Version 62 of these tables.
[h]Spectral response and current-voltage curve reported in Version 60 of these tables.
[i]Stabilised at the manufacturer to the 2% level following IEC procedure of repeated measurements.
[j]Spectral response and/or current-voltage curve reported in Version 46 of these tables.
[k]Spectral response and current-voltage curve reported in Version 55 of these tables.

TABLE 6 | Terrestrial concentrator cell and module efficiencies measured under the ASTM G-173-03 direct beam AM1.5 spectrum at a cell temperature of 25°C (except where noted for the hybrid and luminescent modules).

Classification	Effic. (%)	Area (cm^2)	Intensity[a] (suns)	Test Centre (date)	Description
Single Cells					
GaAs	30.8 ± 1.9[b,c]	0.0990 (da)	61	NREL (1/22)	NREL, 1 junction (1 J)
Si	27.6 ± 1.2[d]	1.00 (da)	92	FhG-ISE (11/04)	Amonix back-contact [76]
CIGS (thin-film)	23.3 ± 1.2[b,e]	0.09902 (ap)	15	NREL (3/14)	NREL [77]
Multijunction cells					
AlGaInP/AlGaAs/GaAs/GaInAs(3) (2.15/1.72/1.41/1.17/0.96/0.70 eV)	47.1 ± 2.6[b,f]	0.099 (da)	143	NREL (3/19)	NREL, 6J inv. metamorphic [62]
GaInP/GaInAs; GaInAsP/GaInAs	47.6 ± 2.6[b,g]	0.0452 (da)	665	FhG-ISE (5/22)	FhG-ISE 4J bonded [78]
GaInP/GaAs/GaInAs/GaInAs	45.7 ± 2.3[b,h]	0.09709 (da)	234	NREL (9/14)	NREL, 4J monolithic [79]
InGaP/GaAs/InGaAs	44.4 ± 2.6[i]	0.1652 (da)	302	FhG-ISE (4/13)	Sharp, 3J inverted metamorphic [80]
GaInAsP/GaInAs	35.5 ± 1.2[b,j]	0.10031 (da)	38	NREL (10/17)	NREL 2-junction (2J) [81]
Minimodule					
GaInP/GaAs; GaInAsP/GaInAs	43.4 ± 2.4[b,k]	18.2 (ap)	340[l]	FhG-ISE (7/15)	Fraunhofer ISE 4J (lens/cell) [82]
Submodule					
GaInP/GaInAs/Ge; Si	40.6 ± 2.0[k]	287 (ap)	365	NREL (4/16)	UNSW 4J split spectrum [83]
Modules					
Si	20.5 ± 0.8[b]	1875 (ap)	79	Sandia (4/89)[l]	Sandia/UNSW/ENTECH (12 cells) [84]
Three Junction (3J)	35.9 ± 1.8[m]	1092 (ap)	N/A	NREL (8/13)	Amonix [85]
Four Junction (4J)	38.9 ± 2.5[n]	812.3 (ap)	333	FhG-ISE (4/15)	Soitec [86]
Hybrid Module[o]					
4-Junction (4J)/bifacial c-Si	34.2 ± 1.9[b,o]	1088 (ap)	CPV/PV	FhG-ISE (9/19)	FhG-ISE (48/8 cells; 4T) [87]
'Notable exceptions'					
Si (large area)	21.7 ± 0.7	20.0 (da)	11	Sandia (9/90)[l]	UNSW laser grooved [88]

(Continues)

TABLE 6 | (Continued)

Classification	Effic. (%)	Area (cm^2)	Intensity[a] (suns)	Test Centre (date)	Description
Luminescent Minimodule[o]	7.1 ± 0.2	25 (ap)	2.5[p]	ESTI (9/08)	ECN Petten, GaAs cells [89]
4 J Minimodule	41.4 ± 2.6[b]	121.8 (ap)	230	FhG-ISE (9/18)	FhG-ISE, 10 cells [90]

Note: Following the normal convention, efficiencies calculated under this direct beam spectrum neglect the diffuse sunlight component that would accompany this direct spectrum. These direct beam efficiencies need to be multiplied by a factor estimated as 0.8746 to convert to thermodynamic efficiencies [91]. Four-terminal module with external dual-axis tracking. Power rating of CPV follows IEC 62670-3 standard, front power rating of flat plate PV based on IEC 60904-3, 60904-5, 60904-7, 60904-10, and 60891 with modified current translation approach; rear power rating of flat plate PV based on IEC TS 60904-1-2 and 60891.

Abbreviations: (da), designated illumination area; (ap), aperture area; CIGS, $CuInGaSe_2$; Effic., efficiency; ESTI, European Solar Test Installation; FhG-ISE = Fraunhofer-Institut für Solare Energiesysteme; NREL, National Renewable Energy Laboratory.

[a]One sun corresponds to direct irradiance of 1000 Wm^{-2}.

[b]Not measured at an external laboratory.

[c]Spectral response and current–voltage curve reported in Version 60 of these tables.

[d]Measured under a low aerosol optical depth spectrum similar to ASTM G-173-03 direct [92].

[e]Spectral response and current–voltage curve reported in Version 44 of these tables.

[f]Spectral response and current–voltage curve reported in Version 54 of these tables.

[g]Spectral response and current–voltage curve reported in Version 61 of these tables.

[h]Spectral response and current–voltage curve reported in Version 46 of these tables.

[i]Spectral response and current–voltage curve reported in Version 42 of these tables.

[j]Spectral response and current–voltage curve reported in Version 51 of these tables.

[k]Determined at IEC 62670–1 CSTC reference conditions.

[l]Recalibrated from original measurement.

[m]Referenced to 1000 W/m^2 direct irradiance and 25°C cell temperature using the prevailing solar spectrum and an in-house procedure for temperature translation.

[n]Measured under IEC 62670-1 reference conditions following the current IEC power rating draft 62,670–3.

[o]Thermodynamic efficiency. Hybrid and luminescent modules measured under the ASTM G-173-03 or IEC 60904–3:2008 global AM1.5 spectrum at a cell temperature of 25°C.

[p]Geometric concentration.

cm^2. Finally, an additional table is being introduced for high bandgap cells to encourage accelerated development of possible upper cell candidates in tandem cell stacks.

Highest confirmed '1 Sun' cell and module results are reported in Tables 1–5. Any changes in the tables from those previously published [1] are set in bold type. In most cases, a literature reference is provided that describes either the result reported, or a similar result (readers identifying improved references are welcome to submit to the lead author). Table 1 summarizes the best-reported measurements for '1 Sun' (non-concentrator) single-junction cells and submodules.

Table 2 contains what might be described as 'notable exceptions' for '1 Sun' single-junction cells and submodules in the above category. Although not conforming to the requirements to be recognized as a class record, the devices in Table 2 have notable characteristics that will be of interest to sections of the photovoltaic community, with entries based on their significance and timeliness. To encourage discrimination, the table is limited to nominally 12 entries with the present authors having voted for their preferences for inclusion. Readers who have suggestions for notable exceptions for inclusion into this or subsequent tables are welcome to contact any of the authors with full details. Suggestions conforming to the guidelines will be included on the voting list for a future issue.

Table 3 is the new table in this issue reporting highest confirmed results for cells of high bandgap (> 1.55 eV) and efficiency above 10% (see table heading and footnotes for other requirements). Table 4 (formerly Table 3) was first introduced in Version 49 of these tables and summarizes the growing number of cell and submodule results involving high efficiency, 1-Sun multiple-junction devices (even earlier, reported in Table 1). Table 5 (formerly Table 4) shows the best results for 1-Sun modules, both single- and multiple-junctions, whereas Table 6 shows the best results for concentrator cells and concentrator modules. A small number of 'notable exceptions' are also included in Tables 4–6.

2 | New Results

Twenty-one new results are reported in the present version of these tables. The first new entry reported in Table 1 ('1-Sun cells and submodules') is a new efficiency record of 27.8% for a large area (134-cm^2) n-type silicon cell fabricated by LONGi and measured by the Institute für Solarenergieforschung (ISFH) in January 2025, with the edge region masked to minimize the impact of edge recombination. LONGi refers to the device as a Hybrid Interdigitated-Back-Contact (HIBC) cell, with heterojunction p-type and TOPCon n-type contacts, making it a HTBC cell in our alternative designation. We retain LONGi's 27.4% total area device efficiency reported in the previous version of these tables [1] since representing actual rather than potential efficiency as for the other masked entries in these tables. The second new result in Table 1 is an energy conversion efficiency of 14.1% reported for a 1-cm^2 $Cu_2ZnSnS_ySe_{4-y}$ (CZTSSe) cell fabricated by the Institute of Physics, Chinese Academy of Sciences (IoP/CAS) [11] and measured by the Chinese National Photovoltaic Industry Measurement and Testing Center (NPVM). The third new result [15] is a large increase in efficiency to 26.9% reported

for a 1-cm^2 Pb-halide perovskite solar cell fabricated by Soochow University, China in conjunction with the University of New South Wales, Sydney (UNSW), and the Zhejiang Baima Lake Laboratory Co., Ltd (BaimaLake), also measured by NPVM. The striking feature regarding this result is that it is only very slightly lower than that for the best small-area (0.1-cm^2) result for a perovskite cell reported as a 'notable exception' in Table 2, in contrast to the much larger differences in the past. The final new result [16] in Table 1 is an increase to 23.9% efficiency for a small (19-cm^2) perovskite minimodule involving nine cells in series fabricated by Microquanta and again measured by NPVM.

Four new results are reported in Table 2 (1-Sun 'notable exceptions'). The first two are in the large area Si cell category where a change has been introduced in this issue of the tables. To allow a more direct comparison between the potential of the commercial technologies, they need to be reported on the same area basis, with 'total area' assessed as the most sensible. This has resulted in one notable entry [1] being removed from the tables: 27.3% efficiency for an all-heterojunction interdigitated back contact (HBC) cell fabricated by LONGi and measured by the Institute für Solarenergieforschung (ISFH) in December 2023, with the edge region masked to minimise the impact of edge recombination. Two new impressive results, also formerly eligible but no longer due to edge masking, are 26.7% for a tunnel oxide passivated contact (TOPCon) cell and 27.1% for an all-TOPCon interdigitated back contact (TBC) cell, both fabricated by Jinko Solar and measured by ISFH in February 2025 for cell 'designated illumination areas' over 310 cm^2 in both cases.

The first of the new entries is a small increase to 24.1% efficiency but a large increase in area to 441 cm^2 for a commercial-size passivated emitter and rear (PERC) cell, fabricated by Trina Solar [31] and measured by ISFH. This is the largest and most powerful (10.6-W) cell yet reported in these tables. The second is 26.4% efficiency for a 335-cm2 TOPCon cell also fabricated by Jinko Solar [32] and again measured by ISFH. This displaces the previous 25.9% figure, which was actually a masked (da) efficiency, rather than the total (t) efficiency reported [1]. The final two entries are for cells over 1000 times smaller, echoing two of the new results in Table 1. The first is an efficiency of 15.8% for a 0.2-cm^2 CZTSSe cell fabricated by IoP/CAS [11] and measured by NPVM. The second [15] is an efficiency of 27.3% for a 0.1-cm^2 Pb-halide perovskite solar cell fabricated by Soochow University in conjunction with UNSW

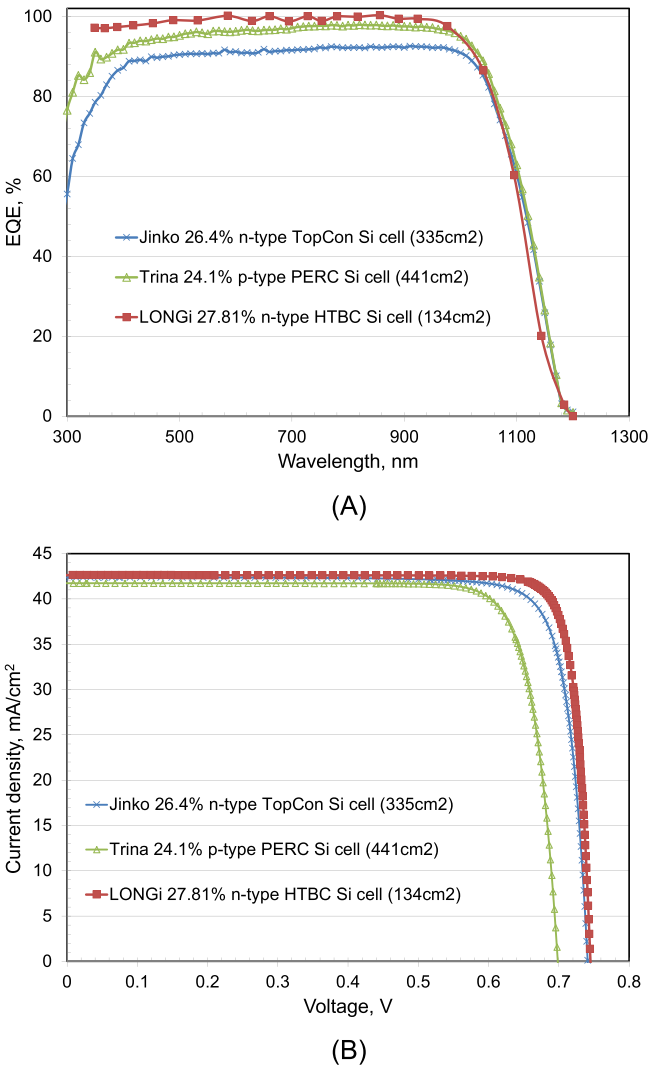

FIGURE 1 | (A) External quantum efficiency (EQE) for the new silicon cell results reported in this issue. (B) Corresponding current density–voltage (JV) curves.

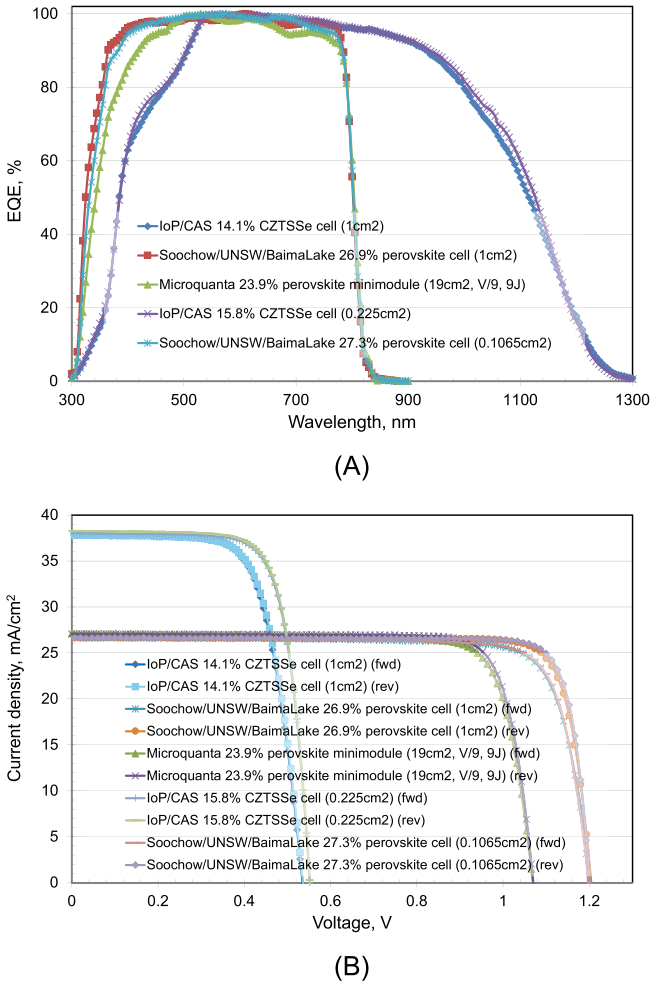

FIGURE 2 | (A) External quantum efficiency (EQE) for new thin-film cell and minimodule results reported in this issue (some curves are normalised). (B) Corresponding current density–voltage (JV) curves.

Sydney and BaimaLake, also measured by NPVM. For these last two results, the cell area is too small for classification as an outright record, with solar cell efficiency targets in governmental research programs generally specified in terms of a cell area of 1-cm^2 or larger [93–95].

Table 3 is new to this issue of the tables and shows entries for high 'effective bandgap' (E_G) cells (>1.55 eV). Such effective bandgaps do not lead to the highest possible efficiencies but are potential candidates for upper cells in tandem cell stacks. One reason for introducing this table is to increase the exposure of results in this area and thereby increase prospects for developing top cell alternatives to perovskites, ideally more stable. Because cell external quantum efficiency (EQE) is available for every certified cell measurement, a procedure with sound underpinnings [96] as described below is used to extract E_G from EQE.

For ideal cells, such as analysed in the classical Shockley–Queisser (SQ) approach, EQE drops abruptly to zero once photon energy falls below E_G, as opposed to actual devices, where the fall-off is gradual. Rau et al. [96] showed actual cells could be regarded conceptually as consisting of a continuous distribution of ideal SQ cells with different E_G. The appropriate distribution is determined by the EQE differential with respect to energy near the absorption edge. Reference [42] shows the spectral EQE for a range of perovskite cells and their energy differential, corresponding to the E_G distribution required to model each cell's absorption edge. As the operative E_G, Rau et al. [96] select the 'mean peak energy', obtained by energy-weighted integration between the two energies where each distribution drops to 50% of peak value. For a symmetrical differential, this will be the energy of the peak value but is shifted slightly if the distribution is skewed [42].

There are seven entries in the new table, three reported in earlier versions of these tables, and four new results, presented in terms of increasing E_G. The first [38] and fourth [41] entries are for Cu (Ga,In)S_2 cells with different Ga/In ratios, with higher E_G than their Se counterparts in Tables 1 and 2, but also lower efficiency of ~15%. A value of over 20% is ultimately feasible and would be ideal for use in tandem stacks. The second [39] and fifth [42] are Pb-halide perovskite solar cells, both representing record performance results at their time of measurement. The third [40] is a record 'pure sulfide' CZTS result featured in Version 65 of these tables. Unfortunately, cell parameters were incorrectly reported in that issue [1] with

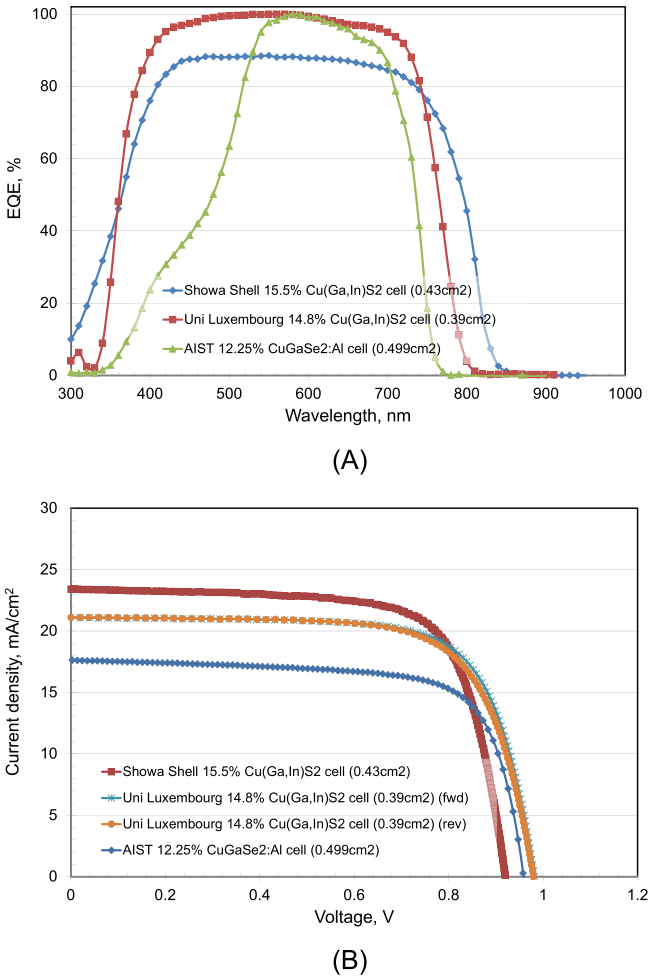

FIGURE 3 | (A) External quantum efficiency (EQE) for three of the new high bandgap cell results reported in this issue (some curves are normalised). (B) Corresponding current density–voltage (JV) curves.

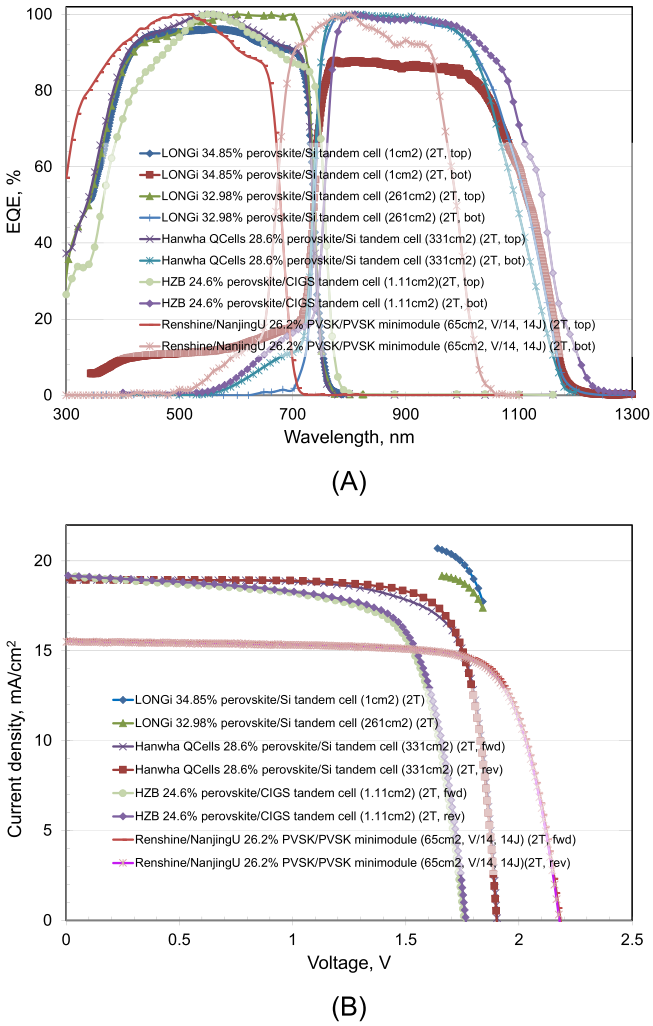

FIGURE 4 | (A) External quantum efficiency (EQE) for new two-terminal double-junction cell and minimodule results reported in this issue (results are normalised). (B) Corresponding current density–voltage (JV) curves.

corrected values shown in bold type. The sixth result [43] is for a 0.5-cm2 CuGaSe2:Al fabricated and measured by the Japanese National Institute of Advanced Industrial Science and Technology [43] (AIST), with the lack of In increasing E_G. The final result [44] is for a crystalline GaInP cell as often used as the top cell in GaAs-based tandem cell stacks, long featured in these tables as a 'notable exception'.

There are five new results reported in Table 4 describing results for 1-Sun, multijunction devices—all involving perovskites in tandem cell stacks. An efficiency of 34.85% is reported for a 1-cm^2, two-terminal, silicon/perovskite tandem cell fabricated by LONGi Central R&D Institute [52], and measured at the US National Renewable Energy Laboratory (NREL) beating out LONGi's earlier 34.6% result [1]. The second is an efficiency of 33.0% for a much larger area (261-cm^2), 2-terminal, silicon/perovskite tandem cell also fabricated by LONGi [53] and measured by NREL on an "aperture area" basis. In keeping with the table's new emphasis on total area results for commercially-sized Si-based cells, another new result is included in this category, 28.6% for a large area (331-cm^2), 2-terminal, silicon/perovskite tandem cell fabricated by Hanwha Qcells [54] and measured by the Fraunhofer Institute for Solar Energy Systems (FhG-ISE) on a 'total area' basis. This equals the efficiency for an earlier result from Oxford PV reported in Version 62, but this time for a larger cell.

The fourth new result in Table 4 is an efficiency of 24.6% measured for a 1-cm^2 perovskite/CIGS monolithic two-junction, two-terminal device, fabricated by Helmholtz Centrum Berlin (HZB) [55] and measured by FhG-ISE, 4% higher than that measured for the best CIGS cell. The final new result in this table in Table 4 is 26.2% efficiency for a 65-cm^2, perovskite/perovskite tandem cell minimodule [57] fabricated by Renshine Solar (Suzhou) Co. Ltd and Nanjing University and measured by the Japan Electrical Safety and Environment Technology Laboratories (JET).

There are four new results reported in Table 5 (1-Sun modules) involving commercially sized silicon and perovskite technologies. The first is a landmark efficiency of 26.0% reported for a 1.8-m^2 silicon module fabricated by LONGi and measured by NREL using the HBC (HJT IBC) cell approach. The second is an efficiency of 25.4% reported for a 1.6-m^2 silicon module fabricated by Trina Solar [64] and measured by FhG-ISE. This equals the efficiency of an earlier module fabricated by LONGi, but uses HJT cell technology, rather than the HBC approach used by LONGi. The third result is improvement to 30.6% efficiency

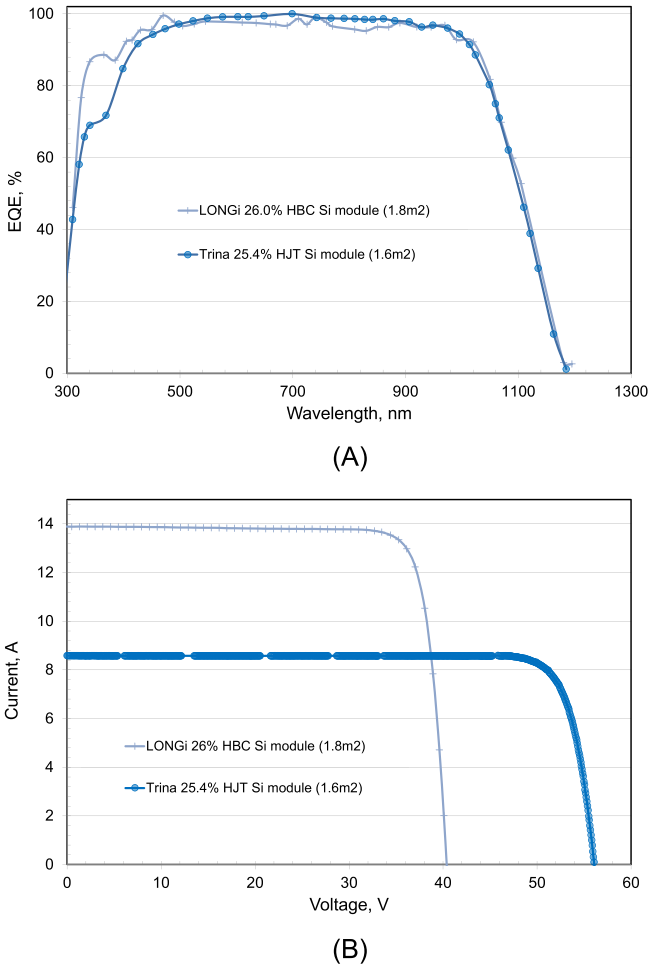

FIGURE 5 | (A) External quantum efficiency (EQE) for the new silicon module results reported in this issue. (B) Corresponding current density–voltage (JV) curves.

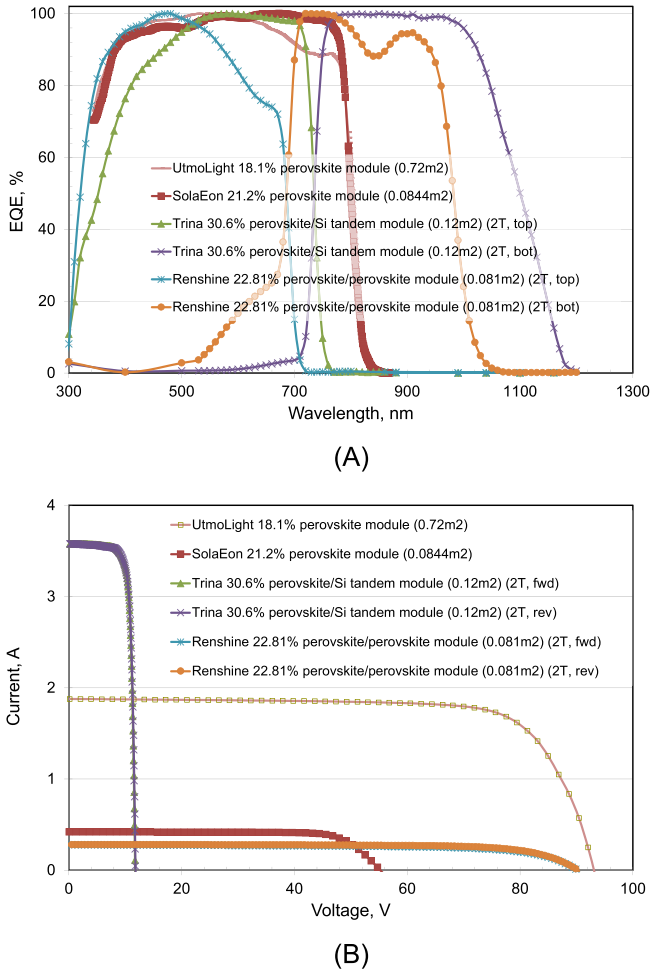

FIGURE 6 | (A) External quantum efficiency (EQE) for the new tandem module and minimodule results reported in this issue. (B) Corresponding current density–voltage (JV) curves.

for a small (0.12-m^2) perovskite/silicon module involving 6 tandem cells fabricated by Trina and measured by FhG-ISE. The second result is improvement to 18.1% efficiency for a 0.72-m^2 perovskite thin-film module [75] fabricated by UtmoLight and measured by NREL.

The EQE spectra for the new silicon cells reported in the present issue of these tables are shown in Figure 1A, with Figure 1B showing the current density–voltage (JV) curves for the same devices. Figure 2A,B show the corresponding EQE and JV curves for several of the new thin-film cell, minimodule and submodule results. Figure 3A,B shows these for three of the new high bandgap cell results, whereas Figure 4A,B shows these for the new two-terminal double-junction tandem cell and minimodule results. Figure 5A,B and Figure 6A,B show these for the new silicon and tandem module results.

Disclaimer

While the information provided in the tables is provided in good faith, the authors, editors and publishers cannot accept direct responsibility for any errors or omissions.

Acknowledgements

The Australian Centre for Advanced Photovoltaics commenced operation in February 2013 with support from the Australian Government through the Australian Renewable Energy Agency (ARENA). The Australian Government does not accept responsibility for the views, information or advice expressed herein. The work at NREL was supported by the U.S. Department of Energy under Contract No. DE-AC36-08-GO28308 with the National Renewable Energy Laboratory. The work at AIST was supported in part by the Japanese New Energy and Industrial Technology Development Organisation (NEDO) under the Ministry of Economy, Trade and Industry (METI). Open access publishing facilitated by University of New South Wales, as part of the Wiley - University of New South Wales agreement via the Council of Australian University Librarians.

Data Availability Statement

The data that support the findings of this study are available from the corresponding author upon reasonable request.

References

1. M. A. Green, E. D. Dunlop, M. Yoshita, et al., "Solar Cell Efficiency Tables (Version 65)," *Progress in Photovoltaics: Research and Applications* 33 (2025): 3–15.

2. M. A. Green, E. D. Dunlop, G. Siefer, et al., "Solar Cell Efficiency Tables (Version 61)," *Progress in Photovoltaics: Research and Applications* 31 (2022): 3–16.

3. M. A. Green, E. D. Dunlop, J. Hohl-Ebinger, et al., "Solar Cell Efficiency Tables (Version 60)," *Progress in Photovoltaics: Research and Applications* 30 (2022): 687–701.

4. https://www.longi.com/en/news/.

5. M. J. Keevers, T. L. Young, U. Schubert, and M. A. Green, "10% efficient CSG minimodules. 22nd European Photovoltaic Solar Energy Conference, Milan," (2007).

6. B. M. Kayes, H. Nie, R. Twist, et al., "27.6% Conversion Efficiency, a New Record for Single-Junction Solar Cells Under 1 Sun Illumination," Proceedings of the 37th IEEE Photovoltaic Specialists Conference, (2011).

7. M, Wanlass, "Systems and Methods for Advanced Ultra-High-Performance In Solar Cells," US Patent 9,590,131 B2, 7 March 2017.

8. M. Nakamura, K. Yamaguchi, Y. Kimoto, Y. Yasaki, T. Kato, and H. Sugimoto, "Cd-free Cu (In,Ga)(Se,S)2 Thin-Film Solar Cell With a New World Record Efficacy of 23.35%, 46th IEEE PVSC, Chicago, IL," June 19, 2019 (see also http://www.solar-frontier.com/eng/news/2019/0117_press.html).

9. R. Diermann, "Avancis Claims 19.64% Efficiency for CIGS Module, PV Magazine International," (2021), https://www.pv-magazine.com/2021/03/04/avancis-claims-19-64-efficiency-for-cigs-module/.

10. "First Solar Press Release, First Solar Builds the Highest Efficiency Thin Film PV Cell on Record," (2014).

11. J. Zhou, X. Xu, H. Wu, et al., "Control of the Phase Evolution of Kesterite by Tuning of the Selenium Partial Pressure for Solar cells With 13.8% Certified Efficiency," *Nature Energy* 8 (2023): 526–535.

12. C. Yan, J. Huang, K. Sun, et al., "$Cu_2ZnSn\ S_4$ Solar cells With Over 10% Power Conversion Efficiency Enabled by Heterojunction Heat Treatment," *Nature Energy* 3 (2018): 764–772.

13. T. Matsui, A. Bidiville, H. Sai, et al., "High-Efficiency Amorphous Silicon Solar cells: Impact of Deposition Rate on Metastability," *Applied Physics Letters* 106 (2015): 053901, https://doi.org/10.1063/1.4907001.

14. H. Sai, T. Matsui, H. Kumagai, and K. Matsubara, "Thin-Film Microcrystalline Silicon Solar cells: 11.9% Efficiency and Beyond," *Applied Physics Express* 11 (2018): 022301.

15. https://www.acap.org.au/post/world-leading-27-perovskite-efficiency-record-achieved-by-unsw-and-soochow-university-with-acap-su.

16. https://www.perovskite-info.com/microquanta-announces-2412-efficiency-1948cm-perovskite-solar-modules.

17. https://www.perovskite-info.com/krict-and-unitest-develop-large-area-perovskite-solar-cell-206-efficiency.

18. L. Han, A. Fukui, Y. Chiba, et al., "Integrated Dye-Sensitized Solar Cell Module With Conversion Efficiency of 8.2%," *Applied Physics Letters* 94 (2009): 013305, https://doi.org/10.1063/1.3054160.

19. R. Komiya, A. Fukui, N. Murofushi, N. Koide, R. Yamanaka, and H. Katayama, "Improvement of the Conversion Efficiency of a Monolithic Type dye-Sensitized Solar Cell Module," Technical Digest, 21st International Photovoltaic Science and Engineering Conference, Fukuoka, November 2011, 2C-5O-08.

20. J. Faisst, E. Jiang, S. Bogati, et al., "Organic Solar Cell with an Active Area > 1 cm2 Achieving 15.8% Certified Efficiency Using Optimized VIS-NIR Anti-Reflection Coating," *Solar RRL* 7 (2023): 2300663.

21. https://www.pv-magazine.com/2021/03/17/organic-pv-module-with-12-36-efficiency/.

22. R. Basu, F. Gumpert, J. Lohbreier, et al., "Large-Area Organic Photovoltaic Modules With 14.5% Certified World Record Efficiency," *Joule* 8 (2024): 970–978.

23. C. C. Boyd, R. Cheacharoen, T. Leijtens, and M. D. McGehee, "Understanding Degradation Mechanisms and Improving Stability of Perovskite Photovoltaics," *Chemical Reviews* 119 (2019): 3418–3451.

24. Y. Yang and J. You, "Make Perovskite Solar Cells Stable," *Nature* 544 (2017): 155–156.

25. U. O. Krašovec, M. Bokalič, and M. Topič, "Ageing of DSSC Studied by Electroluminescence and Transmission Imaging," *Solar Energy Materials and Solar Cells* 117 (2013): 67–72.

26. D. M. Tanenbaum, M. Hermenau, E. Voroshazi, et al., "The ISOS-3 Inter-Laboratory Collaboration Focused on the Stability of a Variety of Organic Photovoltaic Devices," *RSC Advances* 2 (2012): 882–893.

27. (a) F. C. Krebs, ed., *Stability and Degradation of Organic and Polymer Solar cells* (*Wiley, Chichester*, 2012). (b) M. Jorgensen, K. Norrman, S. A.

Gevorgyan, T. Tromholt, B. Andreasen, and F. C. Krebs, "Stability of Polymer Solar cells," *Advanced Materials* 24 (2012): 580–612.

28. M. A. Green, "The Passivated Emitter and Rear Cell (PERC): From Conception to Mass Production," *Solar Energy Materials and Solar Cells* 143 (2015): 190–197.

29. A. Armin Richter, R. Mueller, J. Benick, et al., "Design Rules for High-Efficiency Both-Sides Contacted Silicon Solar cells With Balanced Charge Carrier Transport and Recombination Losses," *Nature Energy* 6 (2021): 429–438.

30. F. Haase, C. Klamt, S. Schäfer, et al., "Laser Contact Openings for Local Poly-Si-Metal Contacts Enabling 26.1%-Efficient POLO-IBC Solar Cells," *Solar Energy Materials and Solar Cells* 186 (2018): 184–193.

31. https://www.pv-magazine.com/2022/07/13/trina-solar-achieves-24-5-efficiency-for-210-mm-p-type-perc-solar-cell/.

32. https://ir.jinkosolar.com/news-releases/news-release-details/jinkosolars-high-efficiency-n-type-monocrystalline-silicon-3.

33. H. Lin, M. Yang, X. Ru, et al., "Silicon Heterojunction Solar Cells With up to 26.81% Efficiency Achieved by Electrically Optimized Nanocrystalline-Silicon Hole Contact Layers," *Nature Energy* 8 (2023): 789–799.

34. "LONGi Achieves New World Record for p-Type Solar Cell Efficiency," Press Release, (2022), https://www.longi.com/en/news/p-type-hjt-record/.

35. K. Keller, K. Kiselman, O. Donzel-Gargand, et al., "High-Concentration Silver Alloying and Steep Back-Contact Gallium Grading Enabling Copper Indium Gallium Selenide Solar Cell with 23.6% Efficiency," *Nature Energy* 9 (2024): 467–478.

36. "First Solar Press Release. First Solar Achieves yet Another Cell Conversion Efficiency World Record," (2016).

37. Y. Ren, D. Zhang, J. Suo, et al., "Hydroxamic Acid Pre-Adsorption Raises the Efficiency of Cosensitized Solar cells," *Nature* 613, no. 7942 (2023): 60–65.

38. H. Hiroi, Y. Iwata, S. Adachi, H. Sugimoto, and A. Yamada, "New World-Record Efficiency for Pure-Sulfide Cu(In,Ga)S2Thin-Film Solar Cell With Cd-Free Buffer Layer via KCN-Free Process," *IEEE Journal of Photovoltaics* 6, no. 3 (2016): 760–763.

39. E. H. Jung, N. J. Jeon, E. Y. Park, et al., "Efficient, Stable and Scalable Perovskite Solar cells Using Poly(3-Hexylthiophene)," *Nature* 567, no. 7749 (2019): 511–515.

40. X. Cui, K. Sun, J. Huang, et al., "Cd-Free Cu2ZnSnS4 Solar Cell With an Efficiency Greater Than 10% Enabled by Al2O3 Passivation Layer," *Energy & Environmental Science* 12 (2019): 2751–2764.

41. D. Adeleye, M. Sood, A. V. Oli, et al., "Wide-Bandgap Cu(In, Ga) S2Solar Cell: Mitigation of Composition Segregation in High Ga Films for Better Efficiency," *Small* 21 (2025): 2405221.

42. M. A. Green and A. W. Y. Ho-Baillie, "Pushing to the Limit: Radiative Efficiencies of Recent Mainstream and Emerging Solar cells," *ACS Energy Letters* 4 (2019): 1639–1644.

43. S. Ishizuka, J. Nishinaga, Y. Kamikawa, T. Nishida, and P. J. Fons, "Photovoltaic Efficiency Enhancement of Indium-Free Wide-Bandgap Chalcopyrite Solar Cells via an Aluminum-Induced Back-Surface Field Effect," *ACS Applied Materials & Interfaces* 17 (2025): 3136–3145.

44. "NREL, private communication," (2019).

45. P. T. Chiu, D. C. Law, R. L. Woo, et al., "35.8% Space and 38.8% Terrestrial 5J Direct Bonded Cells," 2014 IEEE 40th Photovoltaic Specialist Conference (PVSC), Denver, CO, USA, (2014), 0011–0013, https://doi.org/10.1109/PVSC.2014.6924957.

46. K. Sasaki, T. Agui, K. Nakaido, N. Takahashi, R. Onitsuka, and T. Takamoto, "Proceedings, 9th International Conference on Concentrating Photovoltaics Systems, Miyazaki, Japan," (2013).

47. P. Schygulla, R. Müller, O. Höhn, et al., "Wafer-Bonded Two-Terminal III-V//Si Triple-Junction Solar Cell With Power Conversion Efficiency of 36.1% at AM1.5g," Presented at the 40th EU PVSEC, Lisbon, 2023, Paper 2DO.9 (submitted to *Prog. Photovolt. Res. Appl.)*.

48. S. Essig, C. Allebé, T. Remo, et al., "Raising the One-Sun Conversion Efficiency of III–V/Si Solar Cells to 32.8% for Two Junctions and 35.9% for Three Junctions," *Nature Energy* 2 (2017): 17144, https://doi.org/10.1038/nenergy.2017.144.

49. M. Feifel, D. Lackner, J. Schön, et al., "Epitaxial GaInP/GaAs/Si Triple-Junction Solar Cell With 25.9% AM1.5g Efficiency Enabled by Transparent Metamorphic $Al_xGa_{1-x}As_yP_{1-y}$ Step-Graded Buffer Structures," *Solar RRL* 5 (2021): 2000763, https://doi.org/10.1002/solr.202000763.

50. T. J. Grassman, D. J. Chmielewski, S. D. Carnevale, J. A. Carlin, and S. A. Ringel, "GaAs0.75 P0.25/Si Dual-Junction Solar cells Grown by MBE and MOCVD," *IEEE Journal of Photovoltaics* 6 (2016): 326–331.

51. M. A. Green, M. J. Keevers, B. Concha Ramon, et al., "Improvements in Sunlight to Electricity Conversion Efficiency: Above 40% for Direct Sunlight and Over 30% for Global," Paper 1AP.1.2, *European Photovoltaic Solar Energy Conference 2015*, Hamburg, (2015).

52. https://www.longi.com/en/feature-report/world-record-for-solar-cell-efficiency/.

53. https://www.longi.com/en/news/is-m6-wafer-silicon-perovskite-tandem-cells-new-efficiency-record/.

54. https://www.solarpowerworldonline.com/2024/12/qcells-reaches-28-6-efficiency-on-full-size-tandem-perovskite-silicon-solar-cell/.

55. M. Jošt, E. Köhnen, A. Al-Ashouri, et al., "Perovskite/CIGS Tandem Solar Cells: From Certified 24.2% Toward 30% and Beyond," *ACS Energy Letters* 7 (2022): 1298–1307.

56. R. Lin, J. Xu, M. Y. Wei, et al., "All-Perovskite Tandem Solar cells With Improved Grain Surface Passivation," *Nature* 603 (2022): 73–78.

57. H. Gao, K. Xiao, R. Lin, et al., "Homogeneous Crystallization and Buried Interface Passivation for Perovskite Tandem Solar Modules," *Science* 383 (2024): 855–859, https://doi.org/10.1126/science.adj6088.

58. H. Sai, T. Matsui, T. Koida, and K. Matsubara, "Stabilized 14.0%-Efficient Triple-Junction Thin-Film Silicon Solar Cell," *Applied Physics Letters* 109 (2016): 183506, https://doi.org/10.1063/1.49669996.

59. T. Matsui, K. Maejima, A. Bidiville, et al., "High-Efficiency Thin-Film Silicon Solar Cells Realized by Integrating Stable a-Si:H Absorbers Into Improved Device Design," *Japanese Journal of Applied Physics* 54 (2015): 08KB10, https://doi.org/10.7567/JJAP.54.08KB10.

60. M. A. Steiner, R. M. France, J. Buencuerpo, et al., "High Efficiency Inverted GaAs and GaInP/GaAs Solar Cells With Strain-Balanced GaInAs/GaAsP Quantum Wells," *Advanced Energy Materials* 11, no. 4 (2021): 2002874, https://doi.org/10.1002/aenm.202002874.

61. Accessed 28 October 2018, http://mldevices.com/index.php/news/.

62. J. F. Geisz, M. A. Steiner, N. Jain, et al., "Building a Six-Junction Inverted Metamorphic Concentrator Solar Cell," *IEEE Journal of Photovoltaics* 8 (2018): 626–632.

63. K. Makita, Y. Kamikawa, H. Mizuno, et al., "III-V//$Cu_xIn_{1-y}Ga_ySe_2$ Multijunction Solar cells With 27.2% Efficiency Fabricated Using Modified Smart Stack Technology With Pd Nanoparticle Array and Adhesive Material," *Progress in Photovoltaics: Research and Applications* 29 (2021): 887–898, https://doi.org/10.1002/pip.3398.

64. https://www.pv-tech.org/trina-solar-sets-25-44-fully-passivated-hjt-solar-module-efficiency-record/.

65. L. S. Mattos, S. R. Scully, M. Syfu, et al., "New Module Efficiency Record: 23.5% Under 1-Sun Illumination Using Thin-Film Single-Junction GaAs Solar Cells," Proceedings of the 38th IEEE Photovoltaic Specialists Conference, (2012).

66. H. Sugimoto, "High Efficiency and Large Volume Production of CIS-Based Modules," 40th IEEE Photovoltaic Specialists Conference, Denver, (2014).

67. Accessed 28 October 2019, http://www.firstsolar.com/en-AU/-/media/First-Solar/Technical-Documents/Series-6-Datasheets/Series-6-Datasheet.ashx.

68. https://taiyangnews.info/solaeon-technology-announces-world-record-for-perovskite-modules/.

69. M. Hosoya, H. Oooka, H. Nakao, et al., "Organic Thin Film Photovoltaic Modules," Proceedings of the 93rd Annual Meeting of the Chemical Society of Japan, (2013); 21–37.

70. "Sharp Achieves World's Highest Conversion Efficiency of 32.65% in a Lightweight, Flexible, Practically Sized Solar Module," Press Release: June 6, (2022), https://global.sharp/corporate/news/220606-a.html.

71. https://www.oxfordpv.com/news/oxford-pv-debuts-residential-solar-module-record-setting-269-efficiency.

72. J. S. Cashmore, M. Apolloni, A. Braga, et al., "Improved Conversion Efficiencies of Thin-Film Silicon Tandem (MICROMORPH™) Photovoltaic Modules," *Solar Energy Materials and Solar Cells* 144 (2016): 84–95, https://doi.org/10.1016/j.solmat.2015.08.022.

73. V. Bheemreddy, B. J. J. Liu, A. Wills, and C. P. Murcia, "Life Prediction Model Development for Flexible Photovoltaic Modules Using Accelerated Damp Heat Testing," IEEE 7th World Conf. on Photovoltaic Energy Conversion (WCPEC), (2018): 1249–1251.

74. T. Takamoto, H. Juso, K. Ueda, et al., "IMM Triple-junction Solar Cells and Modules optimized for Space and Terrestrial Conditions," Proceedings of the 44th IEEE Photovoltaic Specialist Conference (PVSC), (2017), https://doi.org/10.1109/PVSC.2017.8366097.

75. https://www.pv-magazine.com/2025/03/06/utmolight-pushes-perovksite-pv-module-efficiency-to-18-1/#:~:text=UtmoLight%20has%20reached%2018.1%25%20efficiency,Renewable%20Energy%20Laboratory%20(NREL).

76. A. Slade and V. Garboushian, "27.6% Efficient Silicon Concentrator Cell for Mass Production," Technical Digest, 15th International Photovoltaic Science and Engineering Conference, Shanghai, (2005); 701.

77. J. S. Ward, K. Ramanathan, F. S. Hasoon, et al., "A 21.5% efficient Cu(In,Ga)Se2thin-film concentrator solar cell," *Progress in Photovoltaics: Research and Applications* 10 (2002): 41–46.

78. F. Dimroth, T. N. D. Tibbits, M. Niemeyer, et al., "Four-Junction Wafer-bonded Concentrator Solar Cells," *IEEE Journal of Photovoltaics* 6, no. 1 (2016): 343–349, https://doi.org/10.1109/JPHOTOV.2015.2501729.

79. "NREL Press Release NR-4514," (2014).

80. "Press Release, Sharp Corporation," (2012)," accessed on 5 June 2013, http://sharp-world.com/corporate/news/120531.html.

81. N. Jain, K. L. Schulte, J. F. Geisz, et al., "High-Efficiency Inverted Metamorphic 1.7/1.1 eV GaInAsP/GaInAs Dual-Junction Solar cells," *Applied Physics Letters* 112 (2018): 053905.

82. M. Steiner, G. Siefer, T. Schmidt, M. Wiesenfarth, F. Dimroth, and A. W. Bett, "43% Sunlight to Electricity Conversion Efficiency Using CPV," *IEEE Journal of Photovoltaics* 6, no. 4 (2016): 1020–1024, https://doi.org/10.1109/JPHOTOV.2016.2551460.

83. M. A. Green, M. J. Keevers, I. Thomas, J. B. Lasich, K. Emery, and R. R. King, "40% Efficient Sunlight to Electricity Conversion," *Progress in Photovoltaics: Research and Applications* 23, no. 6 (2015): 685–691.

84. C. J. Chiang and E. H. Richards, "A 20% Efficient Photovoltaic Concentrator Module," *Conf. Record*, 21st IEEE Photovoltaic Specialists Conference, Kissimimee, (1990): 861–863.

85. accessed 23 October 2013, http://amonix.com/pressreleases/amonix-achieves-world-record-359-module-efficiency-rating-nrel-4.

86. S. van Riesen, M. Neubauer, A. Boos, et al., "New Module Design With 4-Junction Solar Cells for High Efficiencies," Proceedings of the 11th Conference on Concentrator Photovoltaic Systems, (2015).

87. J. F. Martínez, M. Steiner, M. Wiesenfarth, G. Siefer, S. W. Glunz, and F. Dimroth, "Power Rating Procedure of Hybrid CPV/PV Bifacial Modules," *Progress in Photovoltaics: Research and Applications* 29 (2021): 614–629.

88. F. Zhang, S. R. Wenham, and M. A. Green, "Large Area, Concentrator Buried Contact Solar cells," *IEEE Transactions on Electron Devices* 42 (1995): 144–149.

89. L. H. Slooff, E. E. Bende, A. R. Burgers, et al., "A Luminescent Solar Concentrator With 7.1% Power Conversion Efficiency," *Physica Status Solidi (RRL)* 2, no. 6 (2008): 257–259.

90. M. Steiner, M. Wiesenfarth, J. F. Martínez, G. Siefer, and F. Dimroth, "Pushing Energy Yield With Concentrating Photovoltaics," *AIP Conference Proceedings* 2149 (2019): 060006, https://doi.org/10.1063/1.5124199.

91. H. Müllejans, S. Winter, M. A. Green, and E. D. Dunlop, "What Is the Correct Efficiency for terrestrial Concentrator PV Devices?," 38th European Photovoltaic Solar Energy Conference, (2021).

92. C. A. Gueymard, D. Myers, and K. Emery, "Proposed Reference Irradiance Spectra for Solar Energy Systems Testing," *Solar Energy* 73 (2002): 443–467.

93. "Program Milestones and Decision Points for Single Junction Thin Films," Annual Progress Report 1984, Photovoltaics, Solar Energy Research Institute, Report DOE/CE-0128, (1985): 7.

94. I. Sakata, Y. Tanaka, and K. Koizawa, "Japan's New National R&D Program for Photovoltaics," Photovoltaic Energy Conversion, Conference Record of the 2006 IEEE 4th World Conference, 1, (2008); 1–4.

95. A. Jäger-Waldau, ed., *PVNET: European Roadmap for PV R&D* (EUR 21087 EN, 2004).

96. U. Rau, B. Blank, T. C. M. Müller, and T. Kirchartz, "Efficiency Potential of Photovoltaic Materials and Devices Unveiled by Detailed-Balance Analysis," *Physical Review Applied* 7 (2017): 044016.